Simplified Remote Measurement of Three-Dimensional Surfaces: Application for Biomedical Engineering

N. Rosenberg†, R. Zeltser, D. Elad, M. Sahar, J. M. Avidor,* and *S. Einav*
Biomedical Engineering Program, Faculty of Engineering, Tel Aviv University, Tel Aviv 69978, Israel

ABSTRACT: Measurement of the topography of biological surfaces, which are often placed in a special liquid environment, is an important need for biomedical investigators. Direct contact measurements are not recommended because any contact with the biological surface may change the delicate mechanical equilibrium and the pattern of the physical phenomenon. This work presents a novel noncontact technique for dynamic visualization and measurement of three-dimensional surfaces of moving boundaries for applications to biomedical studies. The measuring system is simple and is based on innovative image processing procedures. The simplicity of the method enables measurement of surfaces even when the optical path traverses through different media. The validity and accuracy of this new method is investigated on a known cylindrical phantom. A preliminary application to the study of a collapsible tube is demonstrated.

INTRODUCTION

REMOTE SENSING TECHNIQUES which enable non-contact measurement of a complete three-dimensional surface are often required in biomedical engineering. Such measuring techniques are clinically desired in applications where the three-dimensional topography of biological surfaces is needed. Such applications include the design of radiotherapeutic treatments or diagnosis of distorted backs. It is especially essential in biological investigations, *in vitro* or *in vivo* with live bodies or organs, when free space must be ensured around the object under test. In many studies, the application of a dynamic measuring technique will greatly expand the level of biomedical knowledge.

Several photogrammetric methods have been developed or modified to measure and display the three-dimensional topography of irregularly shaped biological surfaces. The most fundamental method is stereography, in which the surface is reconstructed from a pair of images photographed simulataneously by two different cameras (Duncan, 1986). Moiré fringe topography is a grating method that measures with good resolution the contour lines of live objects from which the exact geometry or surfaces can be reconstructed (Meadows *et al.*, 1970; Takasaki, 1973; Yoshino *et al.*, 1976; Pekelsky, 1985). The deficiency of these techniques is in their dependence on the accuracy of the optical components, and, as a result, they are relatively expensive. Rasterstereography is a relatively new and modified stereophotogrammetric technique which overcomes some of the optical deficiencies (Frobin and Hierholzer, 1981, 1983). The measured surface is projected with a raster from an arbitrary angle and the screened image is photographed by a single camera mounted at another arbitrary angle on the opposite side. The complete three-dimensional geometry of the measured surface is constructed by using photogrammetric principles, the direct linear transformation (Abdel-Aziz and Karara, 1971), and control surfaces marked with known points. In this technique, any single image of the surface contains all three-dimensional information; however, many control points are used which require relatively lengthy computations.

All the existing measuring techniques are based on photogrammetric principles and assume that a single medium separates the object from the measuring apparatus (camera and optical accessories). The mathematical formulation used in these techniques draws on the fact that the optical path, traversing through s single medium, consists of straight light rays between the light source, object, and camera; no diffraction due to different media is allowed. However, in practice, especially in experimental investigations, it is often required that the object of interest be placed in a special environment which is inconvenient for the regular measuring instrumentation. For example, biomedical studies with physiological vessels or small organs require that the object be placed in a closed chamber under physiological conditions. It is currently possible to develop complicated test chambers with expensive underwater optical equipment. Nevertheless, simplicity and budgetary limitations call for techniques that will enable one to conduct the three-dimensional measurements from outside the chamber in which the object is installed.

Recently, we have developed a simplified rasterstereography technique that avoids the complex mathematical computation of the direct linear transformation and yet yields accurate measurements of three-dimensional surfaces (Elad *et al.*, 1989). Thus, it can be easily applied to measure objects that are embedded in a liquid-filled chamber. The use of a CCD camera along with novel algorithms for image processing largely simplifies the computational procedure required for geometry reconstruction. The use of a TV camera enables dynamic noncontact measurements. In the present paper we represent the image processing procedure and geometric reconstruction of the three-dimensional surfaces. The accuracy of the measured surfaces was examined with a known phantom both in free air and embedded in a transparent liquid-filled test chamber. The measured data were found to be in very good agreement with the actual geometry, with an overall error of two percent, exceeding most of the requirements in clinical diagnosis or biomedical investigations.

MEASURING APPARATUS

The objective of the experimental set-up was to measure the three-dimensional surface of a fluid-filled flexible tube while subjected to negative transmural (internal minus external) pressures. The fluid may be static or flowing through the tube lu-

†Deceased 9 June 1988.

*To whom correspondence should be sent, at Biomedical Engineering Department, Technological Institute, Northwestern University, 2145 Sheridan Road, Evanston, IL 60208-3107.

PHOTOGRAMMETRIC ENGINEERING AND REMOTE SENSING,
Vol. 56, No. 9, September 1990, pp. 1273-1280.

0099-1112/90/5609–1273$03.00/0

men. For this purpose, a flow circuit was constructed with the tube mounted in a rectangular transparent test chamber (Figure 1). Water flow from a constant-head tank enters the flexible tube through a computer-operated flow-adjusting valve, and exits through a second valve into a downstream reservoir. The flexible tube was made of latex and manufactured by dipping; it had an unstressed internal diameter of 25 mm and a wall thickness of 2 mm. The pressure in the water-filled test chamber was controlled by a vertically moving tank. The pressure inside the tube was measured by a movable catheter-tip connected to a pressure transducer.

The measured surface was screened by a raster (grid of parallel lines) that was projected at 90° to the tube axis, and the resulting image was photographed with a CCD-TV camera (National, Model WV-CD20N/C) equipped with a zoom lens and mounted at an angle from the opposite side (Figure 1). The tube was vertically illuminated so that each raster line coincided with the cross-section of the tube taken perpendicular to the tube axis. The photographed images were either recorded on a professional video tape or digitized and directly transferred to the computer for further processing.

The projected raster was coded to simplify the pattern recognition procedure and accelerate the geometry reconstruction. It was generated from parallel lines, 10.75 lines per cm, with equal width for the lines and the spaces between successive lines. The code was obtained by arranging the lines in groups and leaving out a line each 2, 3, ..., 10 lines (figure 1; view B-B). The total number of lines screened on the region of interest was controlled by the zoom lens.

Three control surfaces, made of aluminum, were installed on both sides of the tube (Figure 1; section A-A) and marked with six control points for the calibration and surface reconstruction procedures. Two surfaces were machined to form two parallel stairs with a vertical separation (height) of 20 mm and were installed to the left of the tube. Another surface, made of a strip, was mounted to the right to of the tube so that its upper surface was coplanar with the upper surface on the left side. The width of each surface was 10 mm. They were mounted in the test chamber along the tube so that the lower left surface coincided with the horizontal plane that contains the nominal center-line of the tube.

In the present study, the length of the measured segment was 100 mm of the tube. Thus, the four outer control points were marked to generate a perpendicular grid of 100 by 100 mm (Figure 1; view B-B). The other two points were marked in the middle between the outer points. The projected raster was adjusted so that the first line coincided with the lower (or upper) two control points.

For preliminary studies and evaluation of the present new technique, a cylindrical phantom was manufactured with a diameter of 30 mm. It was mounted between the control surfaces so that its axis coincided with the nominal center-line of the test chamber.

AUTOMATED RECONSTRUCTION OF THREE-DIMENSIONAL SURFACES

The basic assumption of the present development is that the height of the tube surface is small compared with the distance between the tube and the camera (about 1.5 versus 100 cm). Thus, linearity is assumed between the height of the tube surface and its projection on the image plane. Accordingly, linear relationships are assumed between the real dimensions of the tube and the planar dimensions of the geometry-corrected image. This assumption will be justified later. As a result, we have to correct only for distortions caused by optical parallax and the relative angle between the camera and the horizontal plane.

The fully-automated reconstruction of the three-dimensional geometry of the measured surface has been formulated for a CCD camera and performed on a Microvax equipped with an image processor and a color display. The original image was digitized to a 512- by 512-pixel image of 256 grey levels (Plate 1a) using a color video digitizer board (Imaging Technologies, RGB-512). For the geometry reconstruction surface, a spatial coordiante system X,Y,Z was attached to the tube (Figure 1), and a planar coordinate system x,y to the image plane (Figure 1; view C-C).

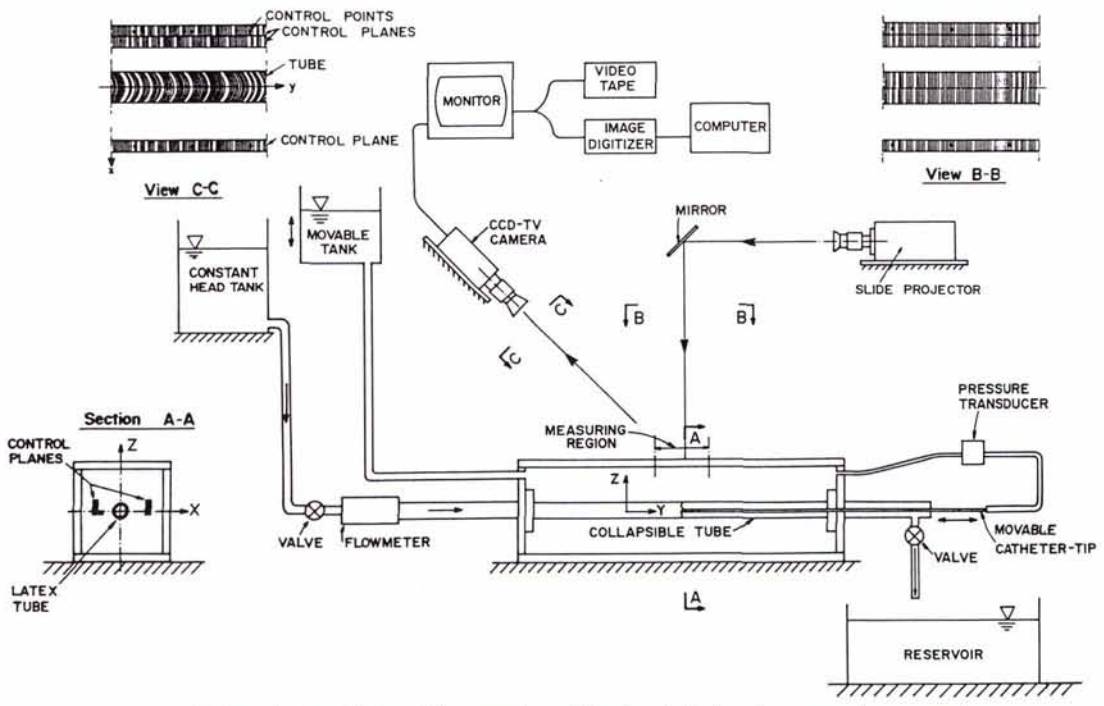

FIG. 1. Schematic description of the experimental setup, including the measuring apparatus.

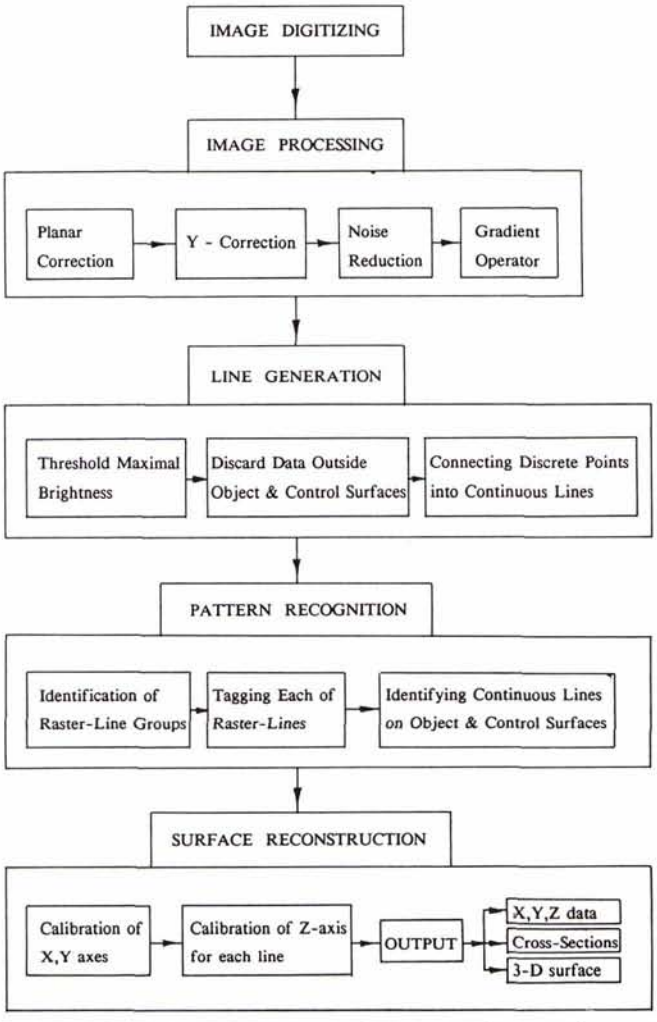

FIG. 2. Flow chart of the automated reconstruction procedure.

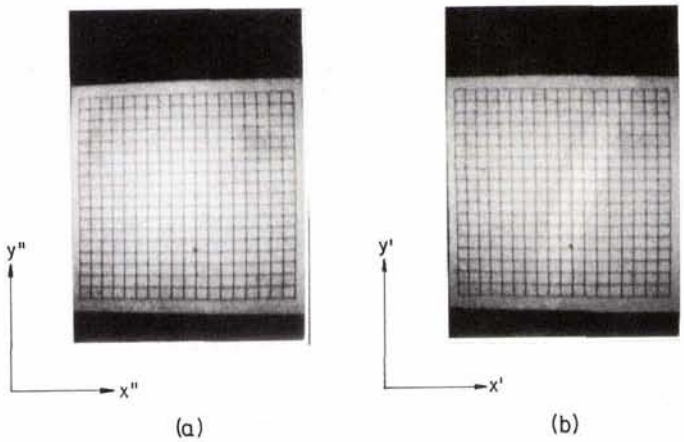

FIG. 3. Straightening procedure of the image of a millimetric chart photographed from above: (a) digitized image; (b) planar-corrected image.

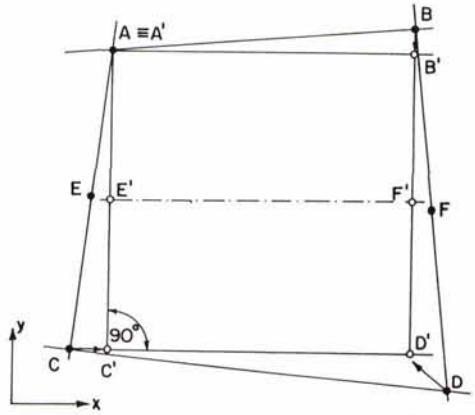

FIG. 4. Geometry-correction by transforming the points A,B,C, and D that originally define a rectangle, to regenerate a rectangle in the image plan.

The computational procedure is composed of several algorithms, which are specially designed for this work (Figure 2). The procedure can be classified according to the following major stages: (1) image processing, (2) line generation, (3) pattern recognition and line identification, and (4) surface reconstruction. Stages (2) and (3) are similar in nature to those described by Frobin and Hierholzer (1983). However, our approach is enhanced due to the coded raster and advanced image processing algorithms used here.

IMAGE PROCESSING

The geometry-correction procedure used to *straighten* the distorted image consists of two phases. First, we applied to the digitized image (Plate 1a) a *planar-correction* algorithm to correct for the distortions usually obtained when an object is photographed from above. Such a distortion, as demonstrated in Figure 3a for a millimetric chart of 180 by 180 mm, may be obtained due to optical parallax and mainly because the camera image plane is not centered above the object. This distortion can be corrected by marking four points on the object so that they create a rectangle. Then, a transformation is imposed on the image of these four control points: A, B, C, and D in Figure 4, to regenerate a rectangle (A', B', C', and D') in the image plane. The rest of the image data are then transformed following the relationship:

$$\begin{pmatrix} x' \\ y' \end{pmatrix} = \begin{pmatrix} a_1 & a_2 & a_3 & a_4 \\ b_1 & b_2 & b_3 & b_4 \end{pmatrix} \begin{pmatrix} x'' \\ x''^2 \\ y'' \\ y''^2 \end{pmatrix} \quad (1)$$

where $(x'',y,'')$ are the original image coordinates and (x',y') are the coordinates of the corrected image. The transformation algorithm is of second order and the eight correction coefficients, a_i and b_i, are computed from the known transformation of the four control points (Figure 4). Once the correction coefficients have been evaluated, one can transfer the whole image through Equation 1 to obtain a straightened image which is again rectangular. Figure 3b demonstrates the straightened image of the original (digitized) image in Figure 3a. The accuracy of this planar-correction procedure can be improved by increasing the number of the correction coefficients and, as a results, the required control points.

In the present measuring apparatus, the inclination between the camera and the tube axis is relatively large (approximately 45°) and, as a result, a greater distortion is obtained, as demonstrated in Figure 5a for the same millimetric chart.

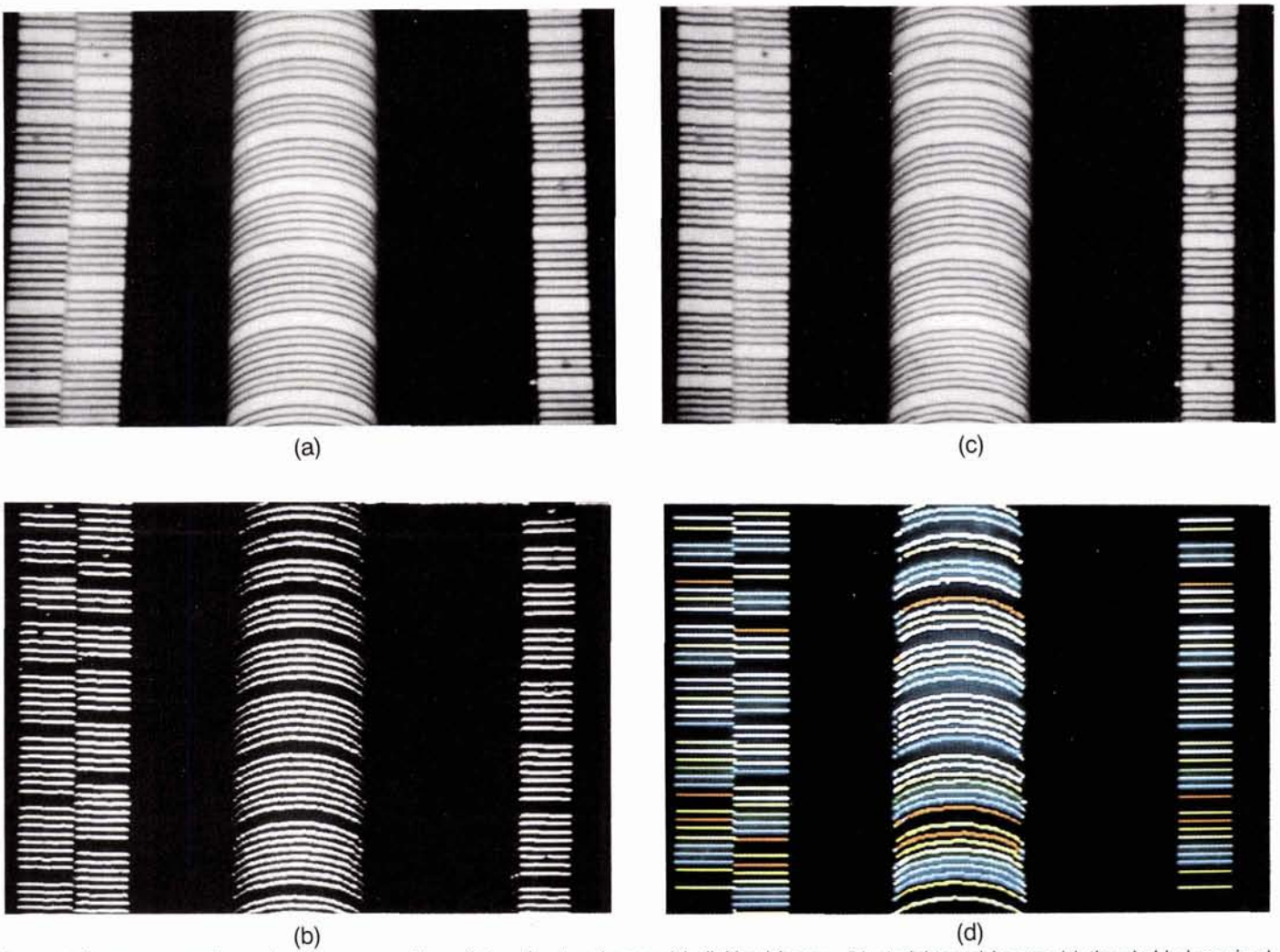

PLATE 1. Image processing and pattern recognition of the phantom image: (a) digitized image; (b) straightened image: (c) thresholded maximal brightness; (d) identified raster lines.

Application of the planar-correction algorithm to the original image (Figure 5a) yields an image (Figure 5b) in which the parallel lines are not equally spaced in the y direction. To correct for this distortion the image was further corrected by adding a *y-correction* procedure which is of the same order and based on the following transformation:

$$x = x'$$
$$y = c_0 + c_1 y' + c_2 y'^2. \quad (2)$$

Here, x',y' are the image data after the first phase of planar-correction,and x,y are the final corrected data that yield the straightened image. The coefficients c_i are computed from three successive control points in the y direction (e.g., A, C, and E in Figure 4). Thus, the complete geometry-correction requires only five control points. For the sake of symmetry, we marked six control points on the upper control surfaces as shown in Figure 1.

The accuracy of the complete geometry-correction procedure was investigated on the millimetric chart (180 by 180 mm) shown in Figure 5, and was found to be within 1 pixel for an image displayed on approximately 450 by 450 pixels. Application of the complete geometry-correction procedure to the original image of the phantom provides the straightened images as shown in Plate 1b.

Following the geometry-correction procedure, we applied conventional image processing methods for noise reduction in the digitized image. Large noises were reduced by passing the geometry-corrected image through a variable 3 by 3 window. The resolution was increased by filtering the data only in the x direction. Then, a gradient algorithm was used to compute the gradients of grey level at each pixel. It consisted of a two-dimensional gradient operator that generated a new image representing the local brightness derivative.

LINE GENERATION

The straightened and processed image is a 512 by 512 matrix describing various grey levels. The measured segment of the tube may be screened with a sequence of lines of the coded raster, that includes groups from 2 up to 10 lines (Maximum 54 lines). Because the lines in the straightened image are equally spaced, the averaged width of a line and its successive space occupy at least about 8 to 9 pixels. Figure 6a demonstrates the brightness distribution across the lines (y direction) for a fixed x. However, for the computational procedure it is necessary to replace the processed image with discrete data that define continuous lines rather than grey band that occupy 4 to 5 pixels. Because the raster was made of equally spaced lines, we choose the maximum brightness (positive derivative of grey level) within each 8 to 9 line region to represent a data point on the raster

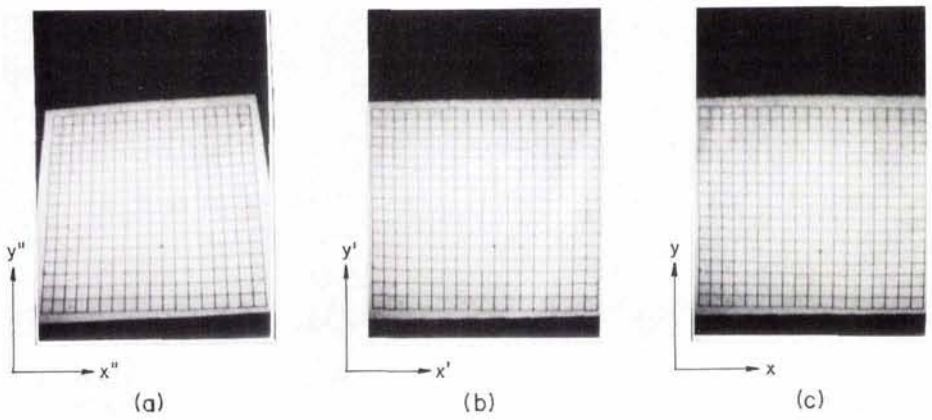

FIG. 5. Straightening procedure of the image of a millimetric chart photographed from an inclination: (a) digitized image; (b) planar-corrected image; (c) y-corrected image.

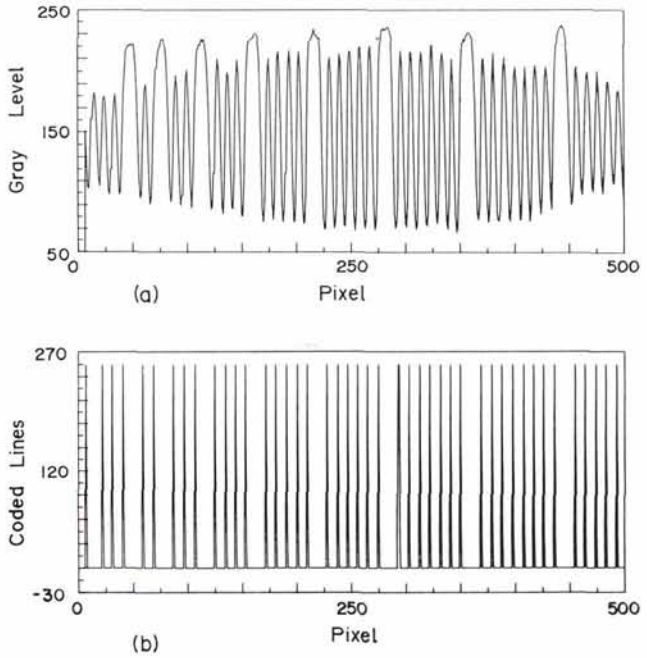

FIG. 6. (a) Distribution of grey levels at a fixed x; (b) The thresholded maximal positive derivative of (a).

line. The vertical (in the y direction) distribution of these maximal derivatives, after a threshold procedure at a fixed x, are represented in Figure 6b. The code of the special designed raster-line is easily recognized.

All the data, except the thresholded maximal brightnesses along y, were then discarded. The remaining data points which were chosen to define the raster lines (the maximal derivatives) constitute a matrix of binary data whose average size is 512 by 45. These data still contain information not required for the present specific application and may be discarded; outside the control surfaces and between the tube and the control surfaces. for this purpose we computed histograms along the y-axis and applied a threshold procedure to define the borders of the tube and the control surfaces. The external borders of the control surfaces are usually very sharp and distinguishable. The internal borders, as obtained by the threshold, can be checked and corrected because the width of the surfaces with respect to their separation is known. The borders of the tube are more smeared due to noise; thus, we added a region of 5 pixels at each side of the tube for further analysis as will be described later.

The data points that belonged to a single raster line (on the tube and on the control surfaces) were then connected to represent continuous lines along the data points. Because most of the data were given on lines that were separated by 7 to 10 pixels, the algorithm searched for close-located points, and also generated missing data points by linear interpolation. In general, no more than 1 to 2 pixels were missing. The data points on the tube were handled from the middle, where the data were clearer, towards both sides. At the boundaries of the tube, where the data were more condensed and 5 pixels were added to the threshold location, the derivatives of the lines were also required to be in the same direction. having defined continuous lines, we discarded all the points between the lines. This procedure was repeated three times to avoid discontinuous lines. At the end of this phase the original image has been transformed into continuous lines. However, there was yet no correlation between the lines on the object (phantom or tube) and on the control surfaces. Representative results of this stage for the phantom are shown in Plate 1c.

Pattern Recognition and Line Identification

A pattern recognition procedure was implemented to identify each of the raster lines on the tube and their continuations on the control surfaces. First, the groups of the coded raster were identified by searching for the wider separations between the lines where lines were removed to encode the raster. For this purpose the histogram in the y direction was computed at a fixed x for all the data being processed. Then, the differences in y between successive lines were histogrammed to evaluate the characteristic deviation between the lines. At the middle of each of the largest deviations we generated the line-code of each group of lines that replaced the lines we had removed to encode the raster. In practice, these lines represent the groups of lines: 2,3,4, etc. of the raster. Once the groups were identified, each line was assigned and tagged for the final calibration. At the end of this stage each of the lines on the measured object and its continuation on the control surfaces is known and stored as a row in the data matrix. Plate 1d shows the already identified lines on the phantom surface with each line represented by a different color.

Surface Reconstruction

Once the x,y values of the projected lines are known in the image plane, one can proceed to the final processing step and compute the actual X,Y,Z, coordinates of the tube surface. Before

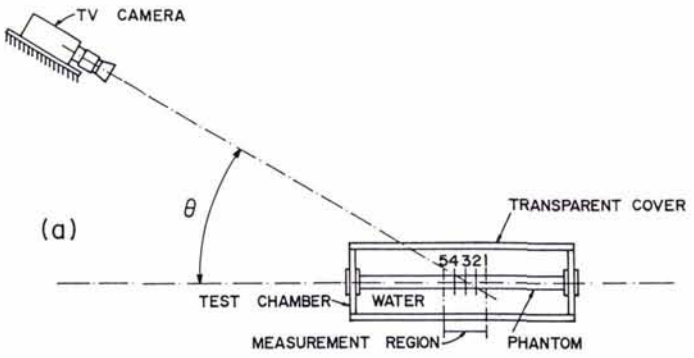

(b)

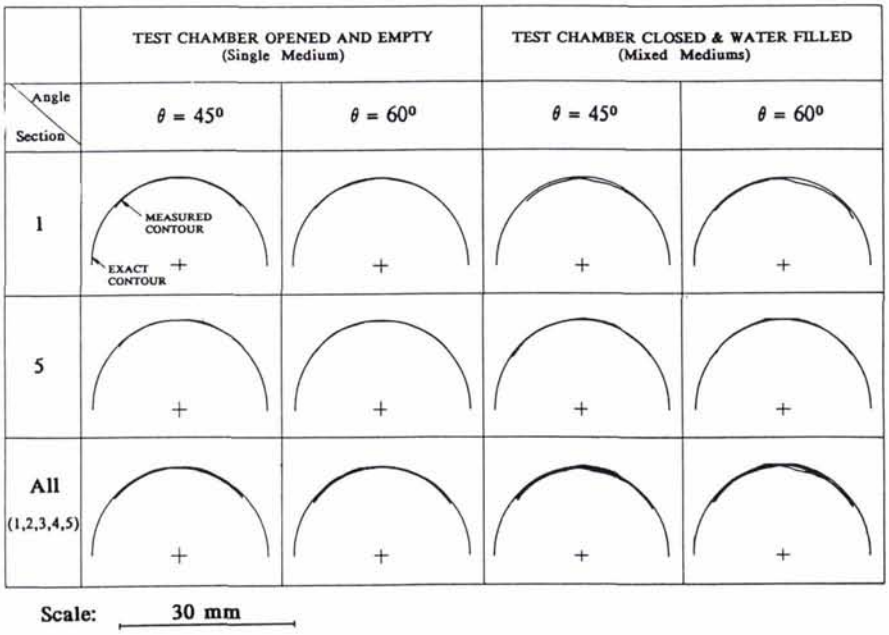

FIG. 7. Comparison between the measured contour and the exact contour of the known cylindrical phantom: (a) schematic description of the relative position between the camera and the tube; (b) measured versus exact contours.

proceeding with data computation, we checked once more the geometry corrections that were performed at the beginning of the automated process. It was assumed that the external border of the left control surface coincided with the vertical y coordinate, and we checked whether the lines on the control surfaces from both sides of the tube are perpendicular to y. The inclination from 90° was then corrected assuming linearity. The distortion was found to be less than 2 pixels.

The evaluation of the actual X,Y,Z coordinates of the tube surface does not follow the usual procedure of rasterstereography methods in which the direct linear transformation (Abdel-Aziz and Karara, 1971) is directly applied to the original image. Up to this point, the data were handled as numbers of pixels in the image plane, rather than dimensional values. In the present work we followed our guidelines that (1) the geometry of the planar projection of the image can be corrected to yield linear relationships between the image x,y coordinates and the actual X,Y coordinates, respectively; and (2) linearity exists between the object height and its geometry-corrected projection on the image plane. Thus, calibration in the X and Y directions was done with the aid of the known control points. The height (Z value) of each point was evaluated by comparing the distortion of each line of the object with the known separations between the left control surfaces. The calibration for Z was performed for each raster line separately. The lower control surface was chosen to be the zero reference for Z.

The real coordinates (X,Y,Z) of each line on the tube represent the actual contour of a cross-section of the tube, because the raster-line was projected on the tube so that it was 90° to the tube axis. The computed data can be now presented as tabulated data, contours of cross-sections, or surface plots, as will be shown later.

ACCURACY EVALUATION AND APPLICATION

A preliminary investigation has been performed to evaluate the validity and accuracy of the present non-contact technique for measuring three-dimensional surfaces. In this study we applied the complete measuring and processing procedure to measure the surface of the known cylindrical phantom. The accuracy of the measured three-dimensional surfaces was investigated with respect to two aspects: (1) the optical path and (2) the inclination between the axes of the camera and the object. For this purpose we measured the phantom with two angles of inclination, $\theta = 45°$ and $\theta = 60°$ (Figure 7a). These measurements were performed once with the phantom placed in the test chamber freely in air, and then with the chamber

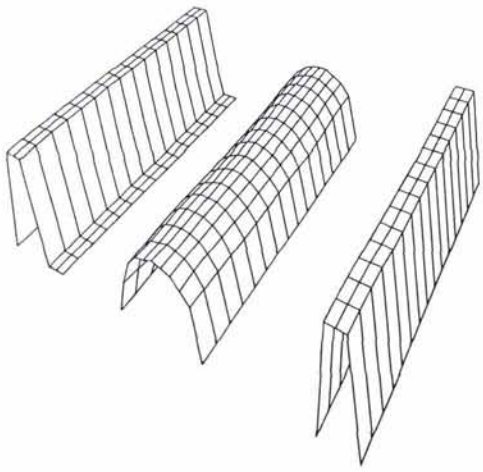

FIG. 8. Three-dimensional reconstruction of the cylindrical phantom and the control surfaces.

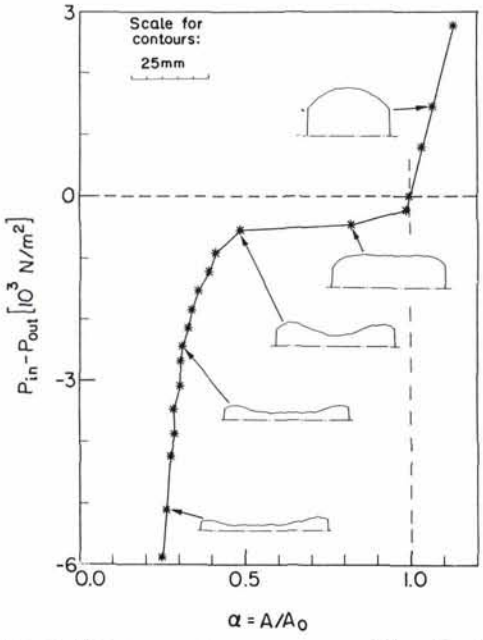

FIG. 9. The measured pressure-area relationship of a latex tube with representative cross-sectional contours. Legend: P_{in} - pressure within the tube, P_{out} - pressure outside the tube, A - cross-sectional area of the tube, and A_o - unstressed cross-sectional area of the tube (at $P_{in}=P_{out}$).

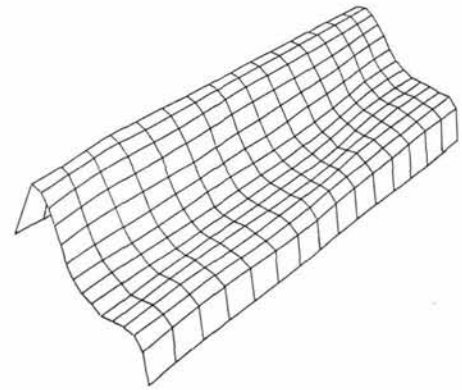

FIG. 10. Three-dimensional reconstruction of the latex tube at a certain collapsed condition.

closed and filled with water. The results of these measurements at different cross-sections along the phantom axis (certain Y locations), in comparison with the exact geometry of the phantom, are summarized in Figure 7b. The calibration factors, for example, for the phantom placed in the closed, water-filled chamber with $\theta=45°$ between the axes of the camera and the tube were 4.12 pixels/mm for X, 4.18 pixels/mm for Y, and 2.70 to 2.75 pixels/mm for Z.

The results of the reconstructed geometry (Figure 7b) are very promising. The measurements with the optical path traversing a single medium (air) are excellent; the maximal deviation between the measured heights (Z) and the real ones is within a single pixel. Thus, the accuracy of the measured height is approximately within the range of one pixel (less than 0.3 mm for the 30-mm diameter cylindrical phantom). The measurements of the phantom embedded in a closed fluid-filled transparent chamber yielded less accurate heights, but still most of the measurements, except for the farthest section (sections 1 and 2), were within a single pixel of the exact values. Accordingly, it has been demonstrated that accurate three-dimensional measurements can also be conducted in cases where the optical path traverses through different media.

The results showed that the accuracy of the present measuring technique is independent of the relative inclination (θ) between the axes of the camera and the object. In addition, the results are also insensitive to tilts of the camera within 5° in the vertical plane generated by the tube axis. To obtain a better resolution, we chose to work with a relative angle of about 45°. The results also show (Figure 7b) that the present technique produces an excellent recontruction of about 110° to 120° of the upper surface of the tube which is seen by the camera. The results are repeatable, and several measurements of the same phantom yield similar results.

One should bear in mind that similar measurements can simultaneously be obtained at about 40 cross-sections along 100 mm of the tube axis. The rest of the information, between the lines, can be calculated by standard interpolation methods, providing an axial accuracy of about 0.25 mm. Thus, a complete three-dimensional surface (Figure 8) is obtained from one single image.

A possible application of this measuring technique in biomedical engineering is in *in vitro* experiments of fluid flow through flexible tubes that simulate several physiological flows. In these studies it is essential to evaluate the mechanical characteristics of the flexible tube which include the relationship between the tube cross-sectional area and the pressure difference across its wall. Figure 9 demonstrates this relationship for a collapsible latex tube as obtained with our simplified measuring system. For the first time, the exact geometry of a collapsible tube was measured at static conditions along with the transmural pressure (internal minus external pressure). At each pressure difference, the tube image was taken and the exact surface reconstructed. Because the whole surface of the measured segment is depicted at once, one can also obtain the complete structure of that segment as shown, for example, in Figure 10.

The measuring procedure can also be used for dynamic measurements of three-dimensional surfaces. It has been demonstrated (Elad *et al.*, 1989; Fig. 5) that a traveling wave can be quantitatively depicted by recording the dynamic event on a video tape. The tape is then replayed and successive images

are processed to yield the exact geometry of the tube as a function of time.

CONCLUSIONS

We have presented a simple technique for dynamic measurement of three-dimensional surfaces. The present method is different from other classical stereophotogrammetric methods with the advantage that it can measure the surface of the object independent of the media the optical path has to traverse. Thus, it can be easily applied to measure objects that are embedded in water-filled chambers. Implementation of modern image processing methods makes the technique powerful, reduces the cost of the optical components, and increases its accuracy. The technique is especially important for measurement of surfaces, such as demonstrated in this work, where a direct contact with the object is prohibited.

ACKNOWLEDGMENTS

This work is dedicated to the memory of Professor Norman Rosenberg who passed away on 9 June 1988. Professor Rosenberg founded the Image Processing Laboratory at Tel Aviv University and the present development was one of the last studies in which he was involved. The paper was edited by Dr. David Elad. This work was supported by the US-Israel Bi-National Science Foundation Grant 84-00348 and the Bat-Sheva de Rothschild Fund for the Advancement of Science and Technology.

REFERENCES

Abdel-Aziz, Y. I., and H. M. Karara, 1971. Direct Linear Transformation from Comparator Coordinates into Object Space coordinates in Close-Range Photogrametry. *Proc. ASP/UI Symp. Close-Range Photogrametry*, Urbana, Illinois, pp. 1–18, American Society of Photogrametry, Falls Church, Virginia.

Duncan, J. P., 1986. Anatomical Definition and Modelling. *Engineering in Medicine*, 15:109–116.

Elad, D., M., Sahar, S., Einav, J. M., Avidor, R., Zeltser, and N., Rosenberg, 1989. A Novel Noncontact Technique for Measuring Complex Surface Shapes Under Dynamic Conditions. *Journal of Physics E: Scientific Instruments*, 22:279–282.

Frobin, W., and E. Hierholzer, 1981. Rasterstereography: A Photogrammetric Method for Measurement of Body Surfaces. *Photogrammetric Engineering & Remote Sensing*, 47:1717–1724.

———, 1983. Automatic Measurement of Body Surfaces Using Rasterstereography (Parts I and II). *Phototgrammetric Engineering & Remote Sensing*, 49:377–384 and 1443–1452.

Meadows, D. M., W. O. Johnson, and J. B. Allen, 1970. Generation of Surface Contours by Moire Topography. *Applied Optics*, 9:942–947.

Pekelsky, J. R., 1985. Automated Contour Ordering in Moire Topograms for Biostereometrics. *Biostereometrics '85*, SPIE, 602:6–17.

Takasaki, H., 1973. Moire Topography. *Applied Optics*, 12:845–850.

Yoshino, Y., M. Tsukiji, and H. Takasaki, 1976. Moire Topography by Means of a Grating Hologram. *Applied Optics*, 155:2414–2417.

(Received 24 May 1989; accepted 28 July 1989; revised 11 December 1989)